Ultrasensitive and broadband MoS₂ photodetector driven by ferroelectrics

Xudong Wang[1,2][†], Peng Wang[1][†], Jianlu Wang[1]*, Weida Hu[1]*, Xiaohao Zhou[1], Nan

Guo[1], Hai Huang[1], Shuo Sun[1], Hong Shen[1], Tie Lin[1], Minghua Tang[2], Lei Liao[3],

Anquan Jiang[4], Jinglan Sun[1], Xiangjian Meng[1], Xiaoshuang Chen[1], Wei Lu[1], Junhao

Chu[1]

[1]National Laboratory for Infrared Physics, Shanghai Institute of Technical Physics,

Chinese Academy of Sciences, 500Yu Tian Road, Shanghai 200083, China

[2]School of Materials Science and Engineering, Xiangtan University, Xiangtan, Hunan

411105, China

[3]Department of Physics and Key Laboratory of Artificial Micro- and Nano-Structures

of Ministry of Education, Wuhan University, Wuhan 430072, China

[4]Department of Microelectronics, Fudan University, 220 Handan Road, Shanghai

200433, China

1

Abstract: Photodetectors based on two dimensional (2D) materials have attracted growing interest. However, the sensitivity is still unsatisfactory even under high gate voltage. Here we demonstrate a MoS_2 photodetector with a poly(vinylidene fluoride-trifluoroethylene) ferroelectric layer in place of the oxide layer in a traditional field effect transistor. The dark current of the photodetector is strongly suppressed by ferroelectric polarization. A high detectivity ($\sim 2.2 \times 10^{12}$ Jones) and photoresponsitivity (2570 A/W) detector has been achieved under ZERO gate bias at a wavelength of 635 nm. Most strikingly, the band gap of few-layer MoS_2 can be tuned by the ultra-high electrostatic field from the ferroelectric polarization. With this characteristic, photoresponse wavelengths of the photodetector are extended into the near infrared (0.85-1.55 μm). A ferroelectrics/optoelectronics hybrid structure is an effective way to achieve high performance 2D electronic/optoelectronic devices.

During the past ten years, because of the unique properties of single layer graphene, two dimensional (2D) materials draw more and more attention for their potential applications in future nanoscale electronic/optoelectronic devices[1-13]. Molybdenum disulfide (MoS_2), consisting of layered S-Mo-S units structures bonded by van der Waals forces, have also been widely studied in recent years[2, 8, 9, 14-17]. MoS_2 is a typical semiconductor with a band gap range from 1.2 eV to 1.8 eV as the thickness decreases from bulk to monolayer[18-20]. Field effect transistors based on monolayer or multilayer MoS_2 possess high current ON/OFF ratios of up to 10^7-10^8 [8, 21-23]. Owing to these special features, ultrathin MoS_2 becomes a promising candidate material for future electronic applications.

For transistors based on 2D graphene and MoS_2, traditional dielectric materials, such as SiO_2, HfO_2, and Al_2O_3, possessing linear dielectric response to an electric field, are usually selected as gate dielectrics[1, 8, 14, 16, 17]. Many interesting and meaningful physical properties have been discovered using these materials. Among these, the optoelectronic properties of a field effect transistor, especially the MoS_2 photodetector (sometimes named a phototransistor) have attracted intensive attention[14-17]. For these photodetectors, the photoresponsivity is relatively low, with the first monolayer MoS_2 phototransistors exhibiting a photoresponsivity of 7.5 mA/W[15]. The specific detectivity D^* for a photodetector, a figure of merit used to characterize performance, is a metric of detector sensitivity. Among these photodetectors, the detectivity is unfavorable for practical applications. Additionally, for these traditional photodetectors, additional gate bias (V_g) and a large drain-source bias (V_{sd}) are essential for obtaining high sensitivity.

3

Such V_g may induce a leakage between source and gate, and the large V_{sd} leads to a significant increase in dark current between the source and drain, as well as a self-heating effect in the channel. These effects will not only cause a large power dissipation, but will also seriously degrade the performance, such as low sensitivity[24, 25]. In recent years, poly(vinylidene fluoride-trifluoroethylene) (P(VDF-TrFE)) ferroelectric polymer films and (lithium niobate) $LiNbO_3$ ferroelectric crystal has been used in nano electronic devices, such as nonvolatile memories[26-31]. In these devices, the function of the ferroelectric film is to tune the transport properties of the channel. However, ferroelectric materials combined with the photoelectric 2D materials have never been used for optoelectronic devices, for example photodetectors.

In this work, the MoS_2 transistor with a ferroelectric gate is used as a photodetector, wherein the few-layer MoS_2 serves as the photosensitive semiconducting channel while the remnant polarization of P(VDF-TrFE) is employed to depress the dark current of the MoS_2 semiconducting channel. The stable remnant polarization can provide an ultra-high local electrostatic field ($\sim 10^9$ V/m within a several nanometer scale) in the semiconductor channel which is larger than that produced by gate bias in traditional field effect transistors[15-17]. With such an ultra-high electrostatic field, the few-layer MoS_2 channel is maintained in a fully depleted state, significantly increasing the sensitivity of the detector even at ZERO gate voltage. Based on these special properties, a photodetector with high detectivity $\sim 2.2 \times 10^{12}$ Jones and photoresponsivity up to 2570 A/W has been achieved. In addition, for the first time the photoresponse wavelengths of the ferroelectric polarization gating MoS_2 photodetector are extended

from the visible to the near infrared (0.85-1.55 μm). Our MoS_2 photodetectors show comparable performances to those of commercial available silicon photodiodes (D^*~ 10^{13} Jones and R ~300 A/W)[32].

A few-layer MoS_2 on a degenerately doped silicon substrate covered with a 285 nm thick silicon oxide was prepared using the Scotch® tape-based mechanical exfoliation method[2, 8]. The molecular configurations of MoS_2 are shown in Fig. 1a. The source and drain chromium (Cr, 5 nm)/gold (Au, 50 nm) electrodes were prepared using the lift-off method. The following step was coating the P(VDF-TrFE) (70:30 in mol%) film as the top gate. The molecular configurations of P(VDF-TrFE) are shown in Fig. 1b respectively. The ferroelectric dipole direction in the P(VDF-TrFE) chain is also shown in Fig. 1b. Then the ultrathin semi-transparent aluminum (~15 nm) electrodes were deposited. The thickness of the few-layer MoS_2 was confirmed by the Raman spectrum (Fig. S1). The peak location of E_{2g}^1 and A_{1g} are 381.32 cm^{-1} and 404.65 cm^{-1}, respectively, and the frequency difference between E_{2g}^1 and A_{1g} vibration modes is 23.27 cm^{-1}. These data correspond to a film thickness of 2.1 nm for the triple-layer MoS_2[18, 19]. The optical image of the whole device based on MoS_2 and P(VDF-TrFE) is shown in Fig. 1c. The three-dimensional device structure schematic view of the ferroelectric polarization gating MoS_2 photodetector with laser beam illumination is shown in Fig. 1d.

Analysis continues with the ferroelectric properties of the P(VDF/TrFE) copolymer being characterized. A typical hysteresis loop for a P(VDF/TrFE) capacitor is shown in Fig. 2a. The thickness of the P(VDF/TrFE) layer is 300 nm. The coercive voltage is

approximately 22.5 V and the remnant polarization value is 7 $\mu C/cm^2$. The polarization switching voltage can be reduced to approximately 5 V with decreasing thickness of the ferroelectric layer[27]. Next, the transfer curves I_{sd}-V_{tg} (drain-source current I_{sd} as a function of top gate voltage V_{tg}) of the MoS_2 transistor with ferroelectric polymer were investigated at room temperature (shown in Fig. 2b). The large memory window (~25 V) in I-V curves between the voltage rise and decrease is related to the ferroelectric polarization switching process. It is more obvious by comparing this curve with the one obtained with the SiO_2 back gate (inset of Fig. 2b). A mobility of $\mu \approx 86.5$ $cm^2V^{-1}s^{-1}$ is calculated from the polymer gated transfer curve using the method in Ref. [8]. The measured transfer characteristics exhibit a typical n type channel FET, showing good agreement with that of a conventional transistor[8]. With the back gate, a mobility of $\mu \approx$ 24.6 $cm^2V^{-1}s^{-1}$ for the few-layer MoS_2 was obtained. The hysteresis behavior is related to the surrounding conditions or the charge transfer from neighboring adsorbates or charge injection into the trap sites on the substrate[33]. The difference in the mobility derived from top or back gates may be associated with the interface nature at the contacts[34, 35]. Based on the ferroelectric polymer/MoS_2 structure, we can achieve three different states: P(VDF/TrFE) without polarization (named as the "fresh" state), polarization up state (P_{up}) and polarization down state (P_{down}). The P_{up} and P_{down} states are achieved by poling P(VDF-TrFE) with -40 V and +40 V. The V_{sd}-I_{sd} characteristics (without additional gate voltage and light illumination) of these three states are shown in Fig. 2c. In the P_{up} state, I_{sd} is the lowest compared to that of the other two states. This situation means that the depleted state of carriers in the MoS_2 channel is caused

6

by the electrostatic field derived from the remnant polarization of P(VDF-TrFE). On the other hand, the P_{down} state corresponds to the accumulated states of carriers in the MoS$_2$ channel. The cross sections of the device structures and equilibrium band diagrams at the different states are shown in Figs. 2d-2f. For a photodetector, the V_{sd}-I_{sd} represents the dark current level without light illumination.

Next, the photoresponse of the MoS$_2$ photodetector was measured at a ZERO gate voltage. The photo switching properties (under V_{sd} = 100 mV) at a wavelength of 635 nm with the three states described above are shown in Fig. 3a. In the fresh state, the signal-to-noise-ratio, photoresponse current (I_{ph}) to dark current (I_{dark}) is very small. In the P_{up} state, a signal-to-noise-ratio of 10^3 is obtained, as can be seen from the photoresponse to pulsed laser illumination curves. In the P_{down} state, I_{ph} cannot be distinguished from the large I_{dark} as the large thermionic and drift/diffusion currents dominate channel current. The results indicate that the electrostatic field produced by the surface charge at the domain surface of P(VDF-TrFE) is strong enough to cause total depletion/accumulation of carriers in the MoS$_2$ semiconducting channel. The domain direction in the ferroelectric material of a charge insufficiently compensated system can be altered by a depolarization field, which leads to the random distribution of ferroelectric domains and, eventually, to the malfunction of the device. (Indeed, before fabricating the ferroelectric layer, we have characterized the photoresponse properties of back gated MoS$_2$ photodetector, as shown in Figure S2. The performance of the traditional back-gate photodetector is very poor compared to the MoS$_2$ photodetector with ferroelectric polarization gating.) For the following measurement,

7

the ferroelectric polarization in P(VDF-TrFE) was preset at a P_{up} state by a short bias pulse of 40 V on the top gate. The I_{sd}-V_{sd} for different illumination powers at a wavelength of 635 nm is shown in Fig. 3b. The I_{sd}-V_{sd} curves, as shown in Fig. 3b, are linear and symmetric. Figure 3c shows the laser power dependence of I_{ph} of the device with V_{sd}=5 V. The inset in Fig.3c is the ratio of I_{ph} to I_{dark} for light on and light off (dark states) at different illumination powers. It can be seen that the device is very sensitive to illumination power. The responsivity (R) of the photodetector is up to 2570 A/W and the detectivity is about ~2.2×10^{12} Jones (under low illumination power 1 nW). The data are extracted from Fig. 3b, where V_{sd} = 5 V and P = 1 nW, given by $R = I_{ph}$ / P, where I_{ph} is the photo current in a detector and P is the illumination power[36, 37]. The value of R (2570 A/W) is larger than previously recorded result ~880 A/W (150 pW, V_{sd}=8 V, and V_g= -70 V)[8]. In addition, the detectivity, assuming that noise from dark current is the major factor, it is given by $D^* = RA^{1/2} / (2eI_d)^{1/2}$, where R is the responsivity, A is the area of the detector, e is the unit charge, and I_d is the dark current[38]. The maximum detectivity ~2.2×10^{12} Jones has been achieved, which is higher than that of detectors based on 2D materials. Note that, if a highly transparent electrode (for example graphene, Ag nano-wire) is chosen, a higher responsivity can be expected. Currently, the transmittance of the available semitransparent Al electrode is only 30% for our device. It suggests that a flawless device fabrication is needed for superior performance in the future.

In addition to the superior sensitivity and good photoresponsivity, we conducted time-resolved photoresponse experiments by periodically turning the illuminating laser on

and off at a frequency of 0.5 Hz and recording the response signal with a high speed oscilloscope (shown in Fig. S3). Fig. 3e shows a complete on/off cycle in which the photocurrent exhibits rapid rise/fall and reaches a steady saturation. The rising and falling edges of the response current are perfectly fitted by a single exponential function. The rise (τ_r) and decay (τ_f) times of the photocurrent, are ~1.8 ms and ~2 ms, respectively, which is relatively fast for state-of-the-art 2D photoconductive photodetectors. In our case, the improvement of response time may result from the interface of P(VDF-TrFE) and MoS_2, the surface trap state of MoS_2 may be encapsulated or passivated by the fluorine or hydrogen atoms from polarized P(VDF-TrFE). Furthermore, the signals recorded by the oscilloscope remain nearly unchanged after 90, 000 cycles of operation (as shown in Fig. 3f), pointing to the excellent stability and reliability of the photodetectors. The stability of the photo-switching behavior is related to the ferroelectric polarization stability of the P(VDF-TrFE) top gate[39, 40] and the reliability of the P(VDF-TrFE)-passivated MoS_2 channel.

All the prominent properties of our photodetector benefit from the ferroelectric-polarization-induced ultra-high electrostatic field of the P(VDF-TrFE). The local electric field at the interface between P(VDF-TrFE) and MoS_2 layers can be estimated from $\sigma = \varepsilon\varepsilon_0 E$, where σ is the charge density at the surface of P(VDF-TrFE) film, which is related to the remnant polarization (P_r) of the ferroelectric materials[27], ε is the dielectric constant of material (the dielectric constant of MoS_2 is approximately 4-6[41, 42], ε_0 is the vacuum permittivity, E is the electric field strength, and P_r is approximately 7.0 $\mu C/cm^2$ calibrated from Fig. 2a. The calculated electric field applied to the triple-

9

layer MoS_2 is about 0.5×10^9 V/m. It is very difficult to obtain such an ultra-high electric field for conventional FETs as described by several research groups[27, 43, 44].

The typical photoresponse spectra of a MoS_2 photodetector is from visible to near infrared (0.85 μm) as the band gap of MoS_2 ranges from 1.2 eV to 1.8 eV. As reported by Oriol Lopez-Sanchez et al., photoresponse is negligible at wavelengths longer than 680 nm (corresponding to one photon energy 1.8 eV) for monolayer MoS_2[14]. For triple-layer MoS_2, the broad absorption tail corresponding to the indirect band transition extends to near 0.85 μm, which is in good agreement with the theoretical prediction[17]. In this work, we also characterized the photoresponse properties of fresh state MoS_2 photodetector, where the response wavelength ends at ~900 nm (shown in Fig. S4). A wider spectral response for a photodetector is important and meaningful. Therefore the response of the detector to light with long wavelength was investigated. The photoresponse of the detector to laser illumination with different wavelengths is shown in Fig. 4a. Surprisingly, it is found that there is still appreciable optical current response to light with wavelength up to 1.55 μm. For the first time, our work broadens the detection of a MoS_2 photodetector from 0.85 μm to 1.55 μm.

To confirm the effect of the electric field polarization on the band structure of few-layer MoS_2, we carried out micro-photoluminescence (PL) measurements on the fresh (ferroelectric domain random) and poled (domain aligned) samples (in Fig. 4b). The PL emission for the pole sample is red-shifted compared to that of the fresh sample, In addition, the PL emission intensity is also increased after the cover of poled P(VDF-TrFE). This effect may be related to the electric field modifying the band structure of

10

the MoS_2 and in turn increasing the density of states of the carriers. With the increase in the carrier population, the radiative recombination of carriers increases, which leads to an increase in PL intensity[45, 46]. Similarly, the band structure of MoS_2 can be tuned by the external strain and confirmed by PL spectrum[45-48]. Note that an optical bandgap measured by PL is different from the bandgap of electron transport due to the exciton binding energy. It has been theoretically predicted that the energy gap of the bi-layer MoS_2 can be tuned by the external electric field[49, 50]. The change in the band-gap in triple-layer MoS_2 under external electric fields applied perpendicular to the layers was also calculated using the density functional theory. The band structure of triple-layer MoS_2 as a function of applied different external electric field is shown in Figs. 4c-e. For example, a 0.40 V/nm of electric field strength can reduce the band gap from 1.09 to 0.71 eV. (Details of the calculation are shown in supplementary information). The indirect bandgap is reduced with an increase of the applied electric field, and the relationship between E_g and electric field is linear (as shown in Fig. S6).

Further studies are needed to clarify the fundamental physics principles of the ferroelectric polarization tuning for the bandgap of few-layer MoS_2. Nevertheless, the ferroelectric/MoS_2 hybrid structure photodetector shows an outstanding performance for detection. Similar electric and photoresponse properties have been also achieved on the same structure with 4-layer MoS_2 photodetector (shown in Fig. S7 and S8). Our photodetector shows a high sensitivity under weak illumination, such as fluorescent lamp (Mov. S1), demonstrating that the few-layer MoS_2 is very promising for a visible to near-infrared digital camera.

11

In summary, we have fabricated the ferroelectric polymer film gated triple-layer MoS_2. The MoS_2 device exhibited outstanding photodetection capabilities compared to traditional MoS_2 FET photodetectors. The device exhibits a maximum attainable photoresponsivity of 2570 A/W, and high detectivity of 2.2×10^{12} Jones, which are record values compared to the previous reports on MoS_2 and other 2D material photodetector. In addition, the broad spectral regions detection, stable and fast photoresponse of the detector are also superior to recently reported MoS_2 photodetectors. The infrared (0.85-1.55 μm) photoresponse of the ferroelectric polarization gating MoS_2 photodetector suggests that such a MoS_2 photodetector is very promising for use in optical communications. The energy gap engineering of a 2D material system combined with an ultra-high ferroelectric-polarization-induced electrostatic field is an attractive research area for next-generation high performance 2D electronic/optoelectronic devices. There are many fruitful and fundamental physics issues in ferroelectric/photoelectric 2D material hybrid systems to be explored in future studies.

Fabrication of the MoS_2 photodetectors.

All measurements were performed under ambient conditions. Triple layers of MoS_2 were exfoliated from commercially available crystals of molybdenite (SPI Supplies brand Moly Disulfide) using the Scotch®-tape micromechanical cleavage technique pioneered for the production of graphene. Triple layers of MoS_2 were deposited on a ~285 nm thick SiO_2 dielectric layer on top of a highly-doped p-type Si wafer

(resistivity$<5\times10^{-3}$ $\Omega\cdot$cm). Electrical contacts were patterned on top of MoS_2 flakes using a conventional lift-off technique. Cr (5 nm) and Au (50 nm) electrodes were deposited by thermal evaporation at room temperature. The device was then annealed at 200 $^\circ$C in a vacuum tube furnace for 2 hours (100 sccm Ar) to remove resist residue and to decrease contact resistance. Then the top gate P(VDF-TrFE) (70:30 mol%) films were prepared by spin coating on the top of the MoS_2. Finally, ultrathin aluminum films were deposited by thermal evaporation as the top gate semi-transparent electrodes.

Characterization of the photodetectors

We performed the electrical and optoelectrical characterization of our device at room temperature using a Lake Shore probe station and Agilent semiconductor parameter analyzer.

In this work, electrical measurements were carried out using an Agilent B2902A, Signal Recovery current preamplifier, lock-in amplifier Signal Recovery 7270 and a current preamplifier Signal Recovery 5182 on the Lake Shore probe station. The photoresponse to laser excitation used a focused λ=500-1550 nm laser beam. A monochrometer was used for wavelength-dependent measurements of the photocurrent. The Raman spectra and PL spectra were acquired by the Lab Ram HR800 from HORIBA (excitation wavelength 532 nm, power 2 mW, spot size 2-3 μm). Time-resolved photoresponse were achieved by high speed the Tektronix MDO3014 Oscilloscope.

Reference

1. Novoselov, K. S. *et al.* Electric field effect in atomically thin carbon films. *Science* **306**, 666–669 (2004).

2. Novoselov, K. S. *et al.* Two–dimensional atomic crystals. *Proc. Natl. Acad. Sci. USA* **102**, 10451–10453 (2005).

3. Nathaniel M. G. *et al.* Hot carrier–assisted intrinsic photoresponse in graphene. *Science* **334**, 648 (2011).

4. Xia, F., Mueller, T., Lin, Y., Valdes–Garcia, A. & Avouris, P. Ultra–fast graphene photodetector. *Nature Nanotech.* **4**, 839–843 (2009).

5. WilliamsJ, R., Dicarlo, L. & Marcus, C. M. Quantum hall effect in a gate–controlled p–n junction of graphene. *Science* **317**, 638 (2007).

6. Yang, H. J. *et al.* Graphene barristor a triode device with a gate–controlled schottky barrier. *Science* **336**, 1140 (2012).

7. Britnell, L. *et al.* Field–effect tunneling transistor based on vertical graphene heterostructures. *Science* **335**, 947 (2012).

8. Radisavljevic, B., Radenovic, A., Brivio, J., Giacometti, V. & Kis, A. Single–layer MoS_2 transistors. *Nature Nanotech.* **6**, 147–150 (2011).

9. Grigorenko, A. N., Polini, M. & Novoselov, K. S. Graphene plasmonics. *Nature Photon.* **6**, 749 (2012).

10. Lee, C. *et al.* Atomically thin p–n junctions with van der waals heterointerfaces. *Nature Nanotech.* **9**, 676–681 (2014).

11. Yuan, H. *et al.* Polarization–sensitive broadband photodetector using a black phosphorus vertical p–n junction. *Nature Nanotech.* (2015).

12. Koppens, F. H. L. *et al.* Photodetectors based on graphene, other two–dimensional materials and hybrid systems. *Nature Nanotech.* **9**, 780–793 (2014).

13. Baugher, B. W. H., Churchill, H. O. H., Yang, Y. & Jarillo–Herrero, P. Optoelectronic devices based on electrically tunable p–n diodes in a monolayer dichalcogenide. *Nature Nanotech.* **9**, 262-267 (2014).

14. Lopez–Sanchez, O., Lembke, D., Kayci, M., Radenovic, A. & Kis, A. Ultrasensitive photodetectors based on monolayer MoS_2. *Nature Nanotech.* **8**, 497−501 (2013).

15. Yin, Z. *et al.* Single–layer MoS_2 phototransistors. *ACS Nano* **6**, 74–80 (2011).

16. Lee, H. S. *et al.* MoS_2 nanosheet phototransistors with thickness-modulated optical energy gap. *Nano Lett.* **12**, 3695−3700 (2012).

17. Choi, W. *et al.* High–detectivity multilayer MoS_2 phototransistors with spectral response from ultraviolet to infrared. *Adv. Mater.* **24**, 5832–5836 (2012).

18. Mak, K. F., Lee, C., Hone, J., Shan, J. & Heinz, T. F. Atomically thin MoS_2: a new direct–gap semiconductor. *Phys. Rev. Lett.* **105**, 136805 (2010).

19. Lee, C. *et al.* Anomalous lattice vibrations of single and few–layer MoS_2, *ACS Nano* **4**, 2695–2700 (2010).

20. Ganatra, R. & Zhang, Q. Few–layer MoS_2: a promising layered semiconductor, *ACS Nano* **8**, 4074–4099 (2014).

21. Liu, H., Neal, A. T. & Ye, P. D. Channel length scaling of MoS_2 MOSFETs. *ACS Nano* **6**, 8563–8569 (2012).

22. Bertolazzi, S., Krasnozhon, D. & Kis, A. Nonvolatile memory cells based on MoS_2/graphene

heterostructures. *ACS Nano* **7**, 3246–3252 (2013).

23. Qiu, H. *et al*. Electrical characterization of back–gated bi–layer MoS$_2$ field–effect transistors and the effect of ambient on their performances. *Appl. Phys. Lett.* **100**, 123104 (2012).

24. Ionescu, A. M. & Riel, H. Tunnel field–effect transistors as energy–efficient electronic switches, *Nature* **479**, 329-337 (2011).

25. Ouyang, Y. & Guo, J. Heat dissipation in carbon nanotube transistors. *Appl. Phys. Lett.* **89**, 183122 (2006).

26. Zheng, Y. *et al*. Graphene field–effect transistors with ferroelectric gating. *Phys. Rev. Lett.* **105**, 166602 (2010).

27. Naber, R. C. G. *et al.* High–performance solution-processed polymer ferroelectric field–effect transistors. *Nature Mater.* **4,** 243-248 (2005).

28. Baeumer, C., Rogers, S. P., Xu, R., Martin, L. W. & Shim, M. Tunable carrier type and density in graphene/PbZr$_{0.2}$Ti$_{0.8}$O$_3$ hybrid structures through ferroelectric switching. *Nano Lett.* **13**, 1693−1698 (2013).

29. Lee, H. S. *et al.* MoS$_2$ nanosheets for top–gate nonvolatile memory transistor channel. *Small* **8**, 3111–3115 (2012).

30. Baeumer, C. *et al.* Ferroelectrically driven spatial carrier density modulation in graphene. *Nature Commun.* **6**, 6136 (2015).

31. Nguyen, A. *et al.* Toward ferroelectric control of monolayer MoS$_2$. *Nano Lett.* **15**, 3364–3369 (2015).

32. Gong, X. *et al.* High–detectivity polymer photodetectors with spectral response from 300 nm to 1450 nm. *Science* **325**, 1665−1667 (2009).

33. Wang, H. *et al.* Hysteresis of electronic transport in graphene transistors. *ACS Nano* **4**, 7221−7228 (2010).

34. Jena, D. & Konar, A. Enhancement of carrier mobility in semiconductor nanostructures by dielectric engineering. *Phys. Rev. Lett.* **98**, 136805 (2007).

35. Fonoberov, V. A. & Balandin, A. A. Giant enhancement of the carrier mobility in silicon nanowires with diamond coating. *Nano Lett.* **6**, 2442–2446 (2006).

36. Konstantatos, G. & Sargent, E. H. Nanostructured materials for photon detection. *Nature Nanotech.* **5**, 391–400 (2010).

37. Guo, Y., Yu, G. & Liu, Y. Functional organic field–effect transistors. *Adv. Mater.* **22**, 4427–4447(2010).

38. Hu, Y. *et al.* Supersensitive, fast-response nanowire sensors by using Schottky contacts. *Adv. Mater.* **22**, 3327−3332 (2010).

39. Kim, W. Y. *et al.* Retention performance of ferroelectric polymer film for nonvolatile memory devices. *IEEE Electron Device Lett.* **30**, 822–824 (2009).

40. Reece, T. J., Gerber, A., Kohlstedt, H. and Ducharme, S. Investigation of state retention in metal–ferroelectric–insulator–semiconductor structures based on Langmuir–Blodgett copolymer films. *J. Appl. Phys.* **108**, 024109 (2010).

41. Chen, X. *et al.* Probing the electron states and metal−insulator transition mechanisms in molybdenum disulphide vertical heterostructures. *Nature Commun.* **6**, 6088 (2015).

42. Santos, E. J. G. & Kaxiras, E. Electrically driven tuning of the dielectric constant in MoS$_2$ layers, *ACS Nano* **7**, 10741–10746 (2013).

43. Gysel, R. *et al.* Retention in nonvolatile silicon transistors with an organic ferroelectric gate. *Appl. Phys. Lett.* **94**, 263507 (2009).

44. Miller, S. L. & McWhorter, P. J. Physics of the ferroelectric nonvolatile memory field effect transistor. *J. Appl. Phys.* **72**, 5999−6010 (1992).

45. Hui, Y. Y. *et al.* Exceptional tunability of band energy in a compressively strained trilayer MoS$_2$ sheet. *ACS Nano* **7**, 7126–7131 (2013).

46. Mouri, S., Miyauchi, Y. & Matsuda, K. Tunable photoluminescence of monolayer MoS$_2$ via chemical doping. *Nano Lett.* **13**, 5944−5948 (2013).

47. Conley, H. J. *et al.* Bandgap engineering of strained monolayer and bilayer MoS$_2$. *Nano Lett.*

13, 3626−3630 (2013).

48. Castellanos−Gomez, A. *et al.* Local strain engineering in atomically thin MoS$_2$. *Nano Lett.* **13**, 5361−5366 (2013).

49. Ramasubramaniam, A., Naveh, D. & Towe, E. Tunable band gaps in bilayer transition−metal dichalcogenides. *Phys. Rev. B* **84**, 205325 (2011).

50. Zibouche, N., Philipsen, P., Kuc, A. & Heine, T. Transition−metal dichalcogenide bilayers: Switching materials for spintronic and valleytronic applications, *Phys. Rev. B* **90**, 125440 (2014).

Acknowledgements

Author contributions

J.W and W.H conceived and supervised the research. X.W and J.W. fabricated the devices. X.W and P.W. performed the measurements. X.Z carried out the calculated part. J.W and W.H wrote the paper. All authors discussed the results and revised the manuscript.

Additional information

Supplementary information is available in the online version of the paper. Correspondence and requests for materials should be addressed to J.W. and W.H.

Competing financial interests

The authors declare no competing financial interests.

Figures
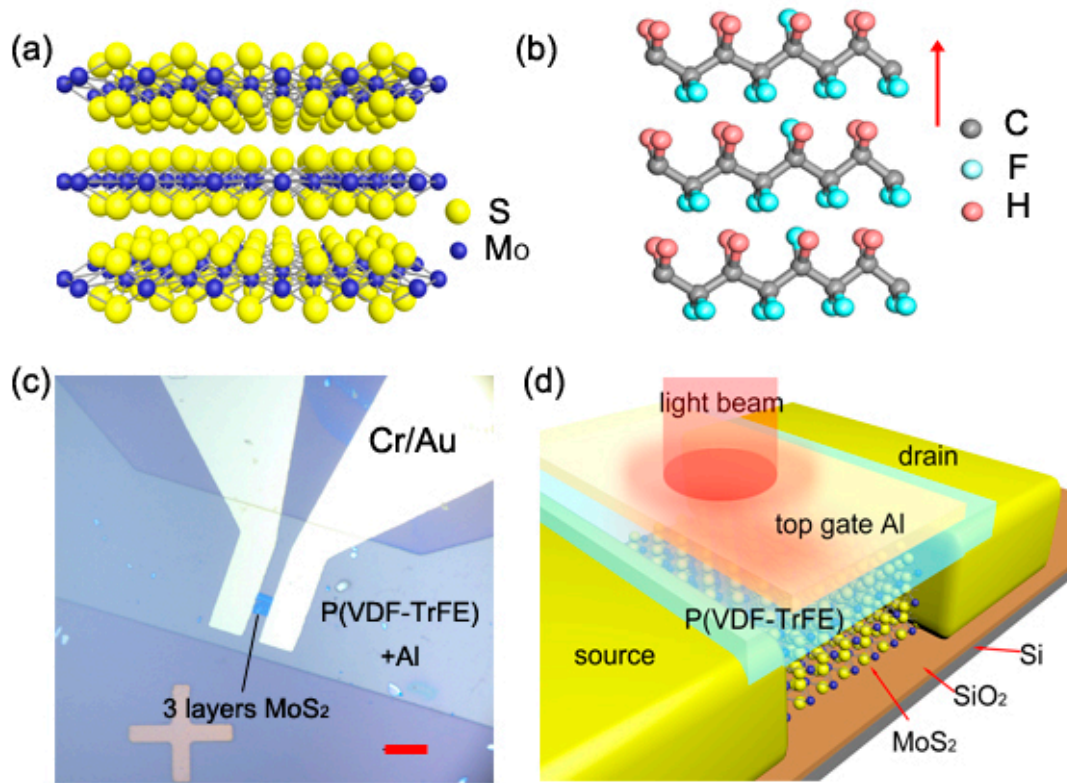
Figure 1. Fabrication and structure of few-layer MoS$_2$ photodetector. a, Schematic structure of triple-layer MoS$_2$. **b**, Schematic structure of P(VDF-TrFE) ferroelectric polymer. The polarization direction of the polymer is pointed out by arrow. **c**, Optical image of the whole device. The device is comprised of triple-layer MoS$_2$ with Cr/Au contract, 250 nm P(VDF-TrFE) ferroelectric polymer and semi-transparent aluminum top electrode. Scale bar, 10μm. **d**, Three dimensional schematic view of the triple-layer MoS$_2$ photodetector with monochromatic light beam.
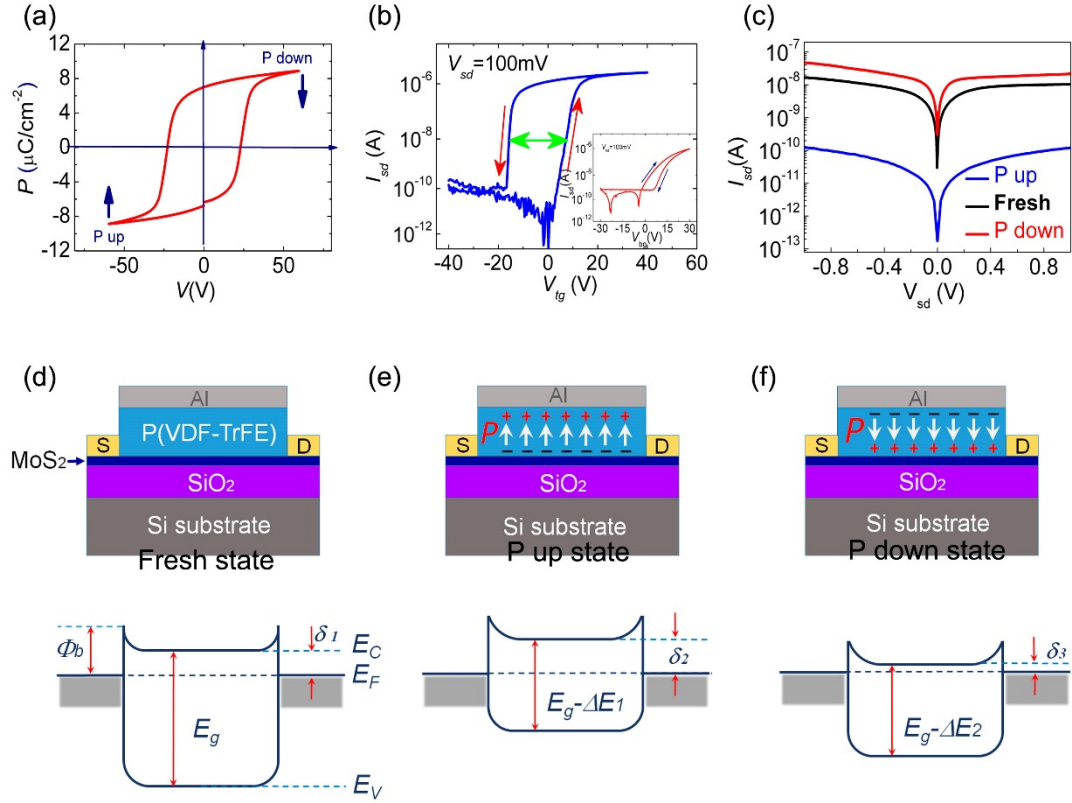
Figure 2. Ferroelectric polarization related electric properties of the P(VDF-TrFE)/MoS₂ hybrid structure. a, The ferroelectric hysteresis loop 300 nm P(VDF-TrFE) film capacitor. It is measured using Sawyer-Tower circuit at 1 Hz applied voltage frequency. **b**, The transfer curves of triple-layer MoS₂ channel with P(VDF-TrFE) ferroelectric polymer gate on dark state at room temperature. The transfer characteristics of triple-layer MoS₂ with SiO₂ back gate are shown in the inset.   **c**, The V_{sd}-I_{sd} characteristics (at ZERO gate voltage) with three states of ferroelectric layer. The three states are: fresh state (ferroelectric layer without polarization), polarization up ("P up", polarized by a pulse V_g of -40 V) and polarization down ("P down", polarized by a pulse V_g of -40 V) states, respectively. **d-f**, The cross section structures of the device and equilibrium energy band diagrams of three different ferroelectric polarization states with V_{sd}=0 V. For the band diagrams of different states, small

19

Schottky barriers at the source and drain electrodes are considered. E_F, E_c E_V, Φ_B, and E_g are the Fermi level energy, minimum conduction band energy, maximum valence band energy, Schottky barrier height and bandgap of MoS_2, respectively. δ is the height from bottom of conduction band to the Fermi level. δ_1, δ_2 and δ_3 are related to the three states.
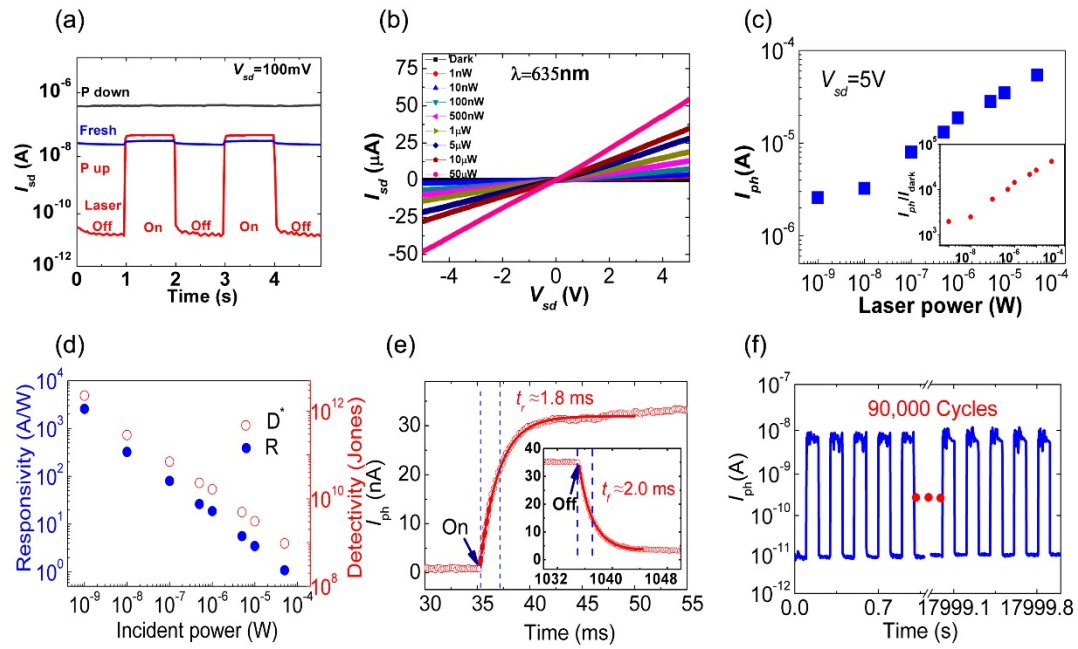
Figure 3. Photoresponse properties of the ferroelectric polarization gating triple-layer MoS₂ photodetector. a, Photoswitching behavior of ferroelectric polarization gating triple-layer MoS$_2$ photodetector at three states (λ=635 nm, V_{sd}=100 mV, P=100 nW). **b,** Drain-source characteristic of the photodetector in the dark and under different illuminating light powers (1nW to 50 μW). **c,** Dependence of photocurrent on illumination powers. Inset is the ratio of photoresponse current to dark current under different illumination powers. **d,** Photoresponsivity of the MoS$_2$ phototransistor, showing high sensitivity. The device exhibits a photoresponsivity of 2570 A/W for an laser power of 1 nW, and the detectivity is up to ~2.2×10^{12} Jones. **e,** The rise and fall of the photocurrent and the fitted data using exponential functions (recorded by V_{sd}=100 mV and P=100 nW). **f,** Photocurrent response during 90,000 cycles of operation at V_{sd}=100 mV and P=100 nW. The device shows an endurable photoresponse.
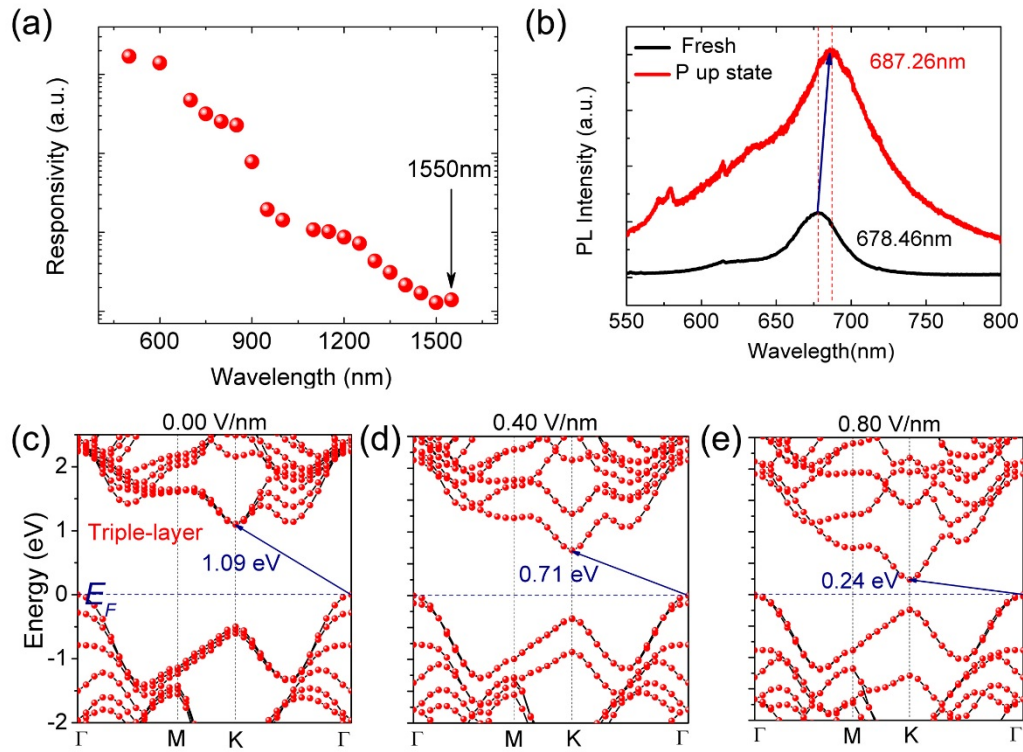
Figure 4. Infrared photoresponse of ferroelectric polarization gating few-layer MoS$_2$ photodetector beyond its intrinsic bandgap. a, Photoresponsitivity of a similar polarization-gating triple layer MoS$_2$ photodetector as a function of light wavelength from 500 nm to 1550 nm at V_{sd}=1 V and P=100 μW). **b,** Comparison photoluminescence spectrum of fresh and polarization gating triple-layer MoS$_2$. **c-e,** The band structures evolution of triple-layer MoS$_2$ under different external electric field (0.0, 0.4, and 0.8 V/nm) by first-principle DFT calculations.

Supplementary Information for

Ultrasensitive and broadband MoS₂ photodetector driven by ferroelectrics

Xudong Wang[1,2][†], Peng Wang[1][†], Jianlu Wang[1]*, Weida Hu[1]*, Xiaohao Zhou[1], Nan Guo[1], Hai Huang[1], Shuo Sun[1], Hong Shen[1], Tie Lin[1], Minghua Tang[2], Lei Liao[3], Anquan Jiang[4], Jinglan Sun[1], Xiangjian Meng[1], Xiaoshuang Chen[1], Wei Lu[1], Junhao Chu[1]

[1]National Laboratory for Infrared Physics, Shanghai Institute of Technical Physics, Chinese Academy of Sciences, 500Yu Tian Road, Shanghai 200083, China

[2]School of Materials Science and Engineering, Xiangtan University, Xiangtan, Hunan 411105, China

[3]Department of Physics and Key Laboratory of Artificial Micro- and Nano-Structures of Ministry of Education, Wuhan University, Wuhan 430072, China

[4]Department of Microelectronics, Fudan University, 220 Handan Road, Shanghai 200433, China

Email: jlwang@mail.sitp.ac.cn, wdhu@mail.sitp.ac.cn

Contents

1. The Raman spectra of triple layer MoS$_2$.

Figure S1. The Raman spectra of triple layer MoS$_2$. The peak position of E_{2g}^1 and A_{1g} are 381.32 cm^{-1} and 404.65 cm^{-1}, respectively. The separation between E_{2g}^1 and A_{1g} modes is approximately 23.27 cm^{-1}.

## 2. Photoresponse properties of back-gated triple-layer MoS₂ photodetector.
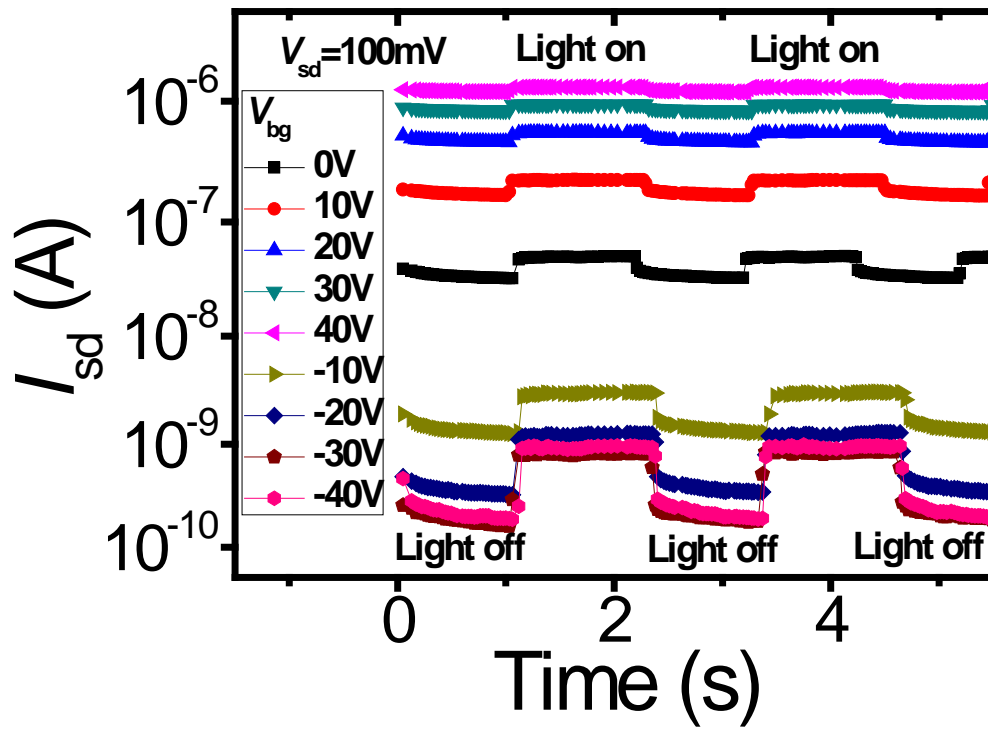
Figure S2. Photoresponse behavior of back-gated triple-layer MoS₂ photodetector with different back gate voltages and V_{sd}=100mV at a wavelength of 635 nm (P=100nW).

3. Time-resolved photoresponse of ferroelectric polarization gating MoS$_2$ photodetector
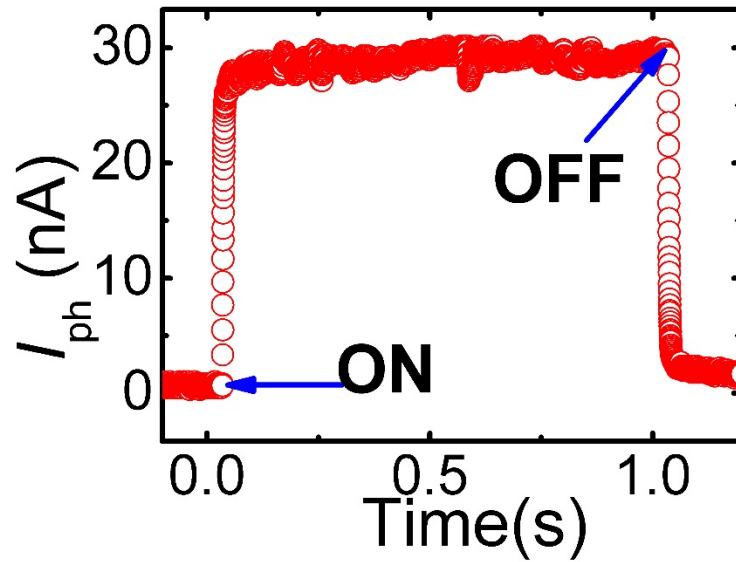
Figure S3. Time-resolved photoresponse of ferroelectric polarization gating MoS$_2$ photodetector. The data are recorded by a high speed oscilloscope at V_{sd}=100mV and P=100nW.

## 4. Photoresponse of tri-layer MoS$_2$ photodetector on fresh state
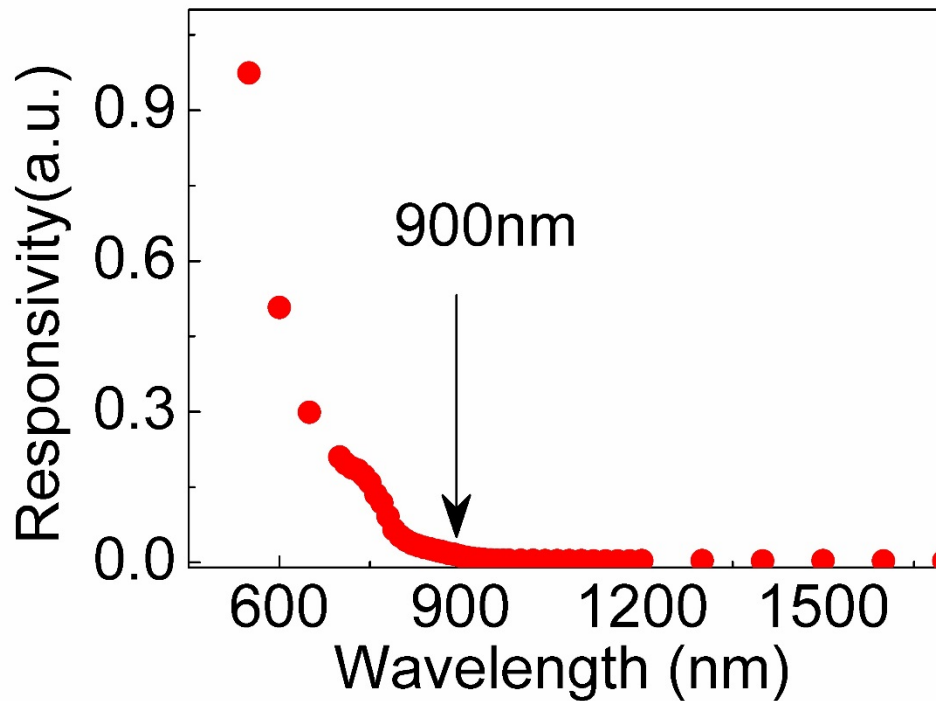
Figure S4. Photoresponsivity of triple-layer MoS$_2$ device (without ferroelectric) as a function of illumination wavelength. The device shows a decreasing responsivity as the illumination wavelength changes from 500 nm to 900 nm. When the wavelength is larger than 900, there is nearly no photoresponse for the device.

5. Calculations on band structures evolution of triple-layer MoS$_2$

The first-principle DFT calculations were performed within the DMol^3 code[S1]. The generalized gradient approximation (GGA) with the Perdew–Burke–Ernzerhof (PBE) function was utilized as the exchange–correlation function[S2]. The DFT-D (D stands for dispersion) approach within the Grimme scheme was adopted for the van der Waals corrections[S3]. DFT Semi-core Pseudopots (DSPP), which induce some degree of relativistic correction into the core, were used for the core treatment. Moreover, double numerical atomic orbital plus polarization was chosen as the basis set, with the global orbital cutoff of 4.6 Å The k-point was set to $7 \times 7 \times 1$ for the structural optimization and $11 \times 11 \times 1$ for the electronic properties calculations, and the smearing value was 0.005 Ha. The convergence tolerances of energy, maximum force, and maximum displacement were set to 1.0×10^{-5} Ha, 0.002 Ha/Å and 0.005 Å respectively. The vacuum length between two adjacent images in the supercell is longer than 15 Å. The external electric field (0 to 1.0 V/nm) was applied in the direction perpendicular to the triple-layer plane, and then geometry relaxation was carried out.

Furthermore, the band gap (E_g) value as a function of electric field is displayed in Figure S6. Clearly. E_g is linearly dependent on electric field with a slope of 1.12. The linear relationship of E_g and electric field was also reported in the transition-metal dichalcogenide bilayers under external electric field[S4].
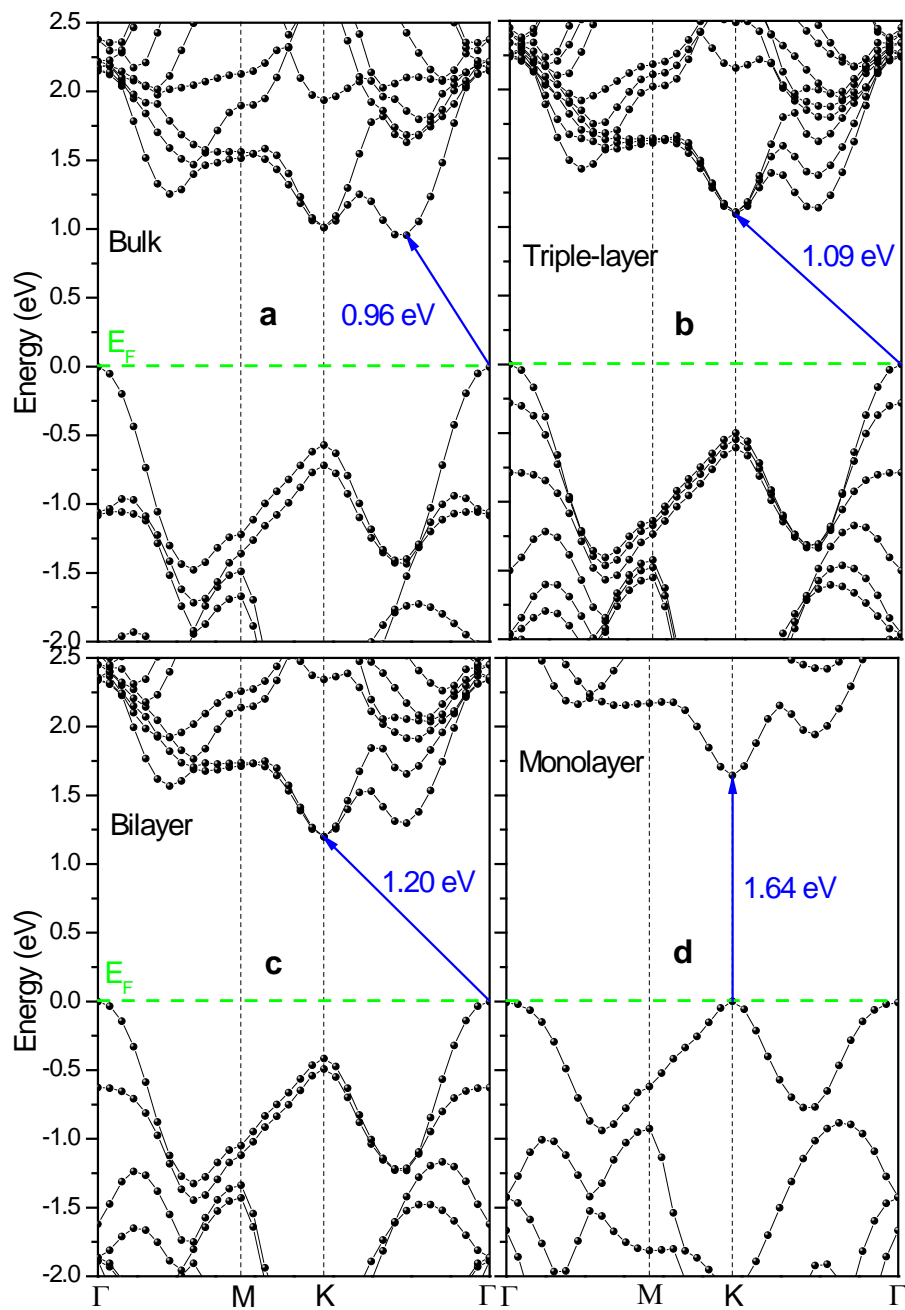
Figure S5. Computed electronic band structures of bulk (a), triple-layer (b), bilayer, and monolayer (d) MoS_2. The Fermi level (E_F) is shifted to the top of the valence band.
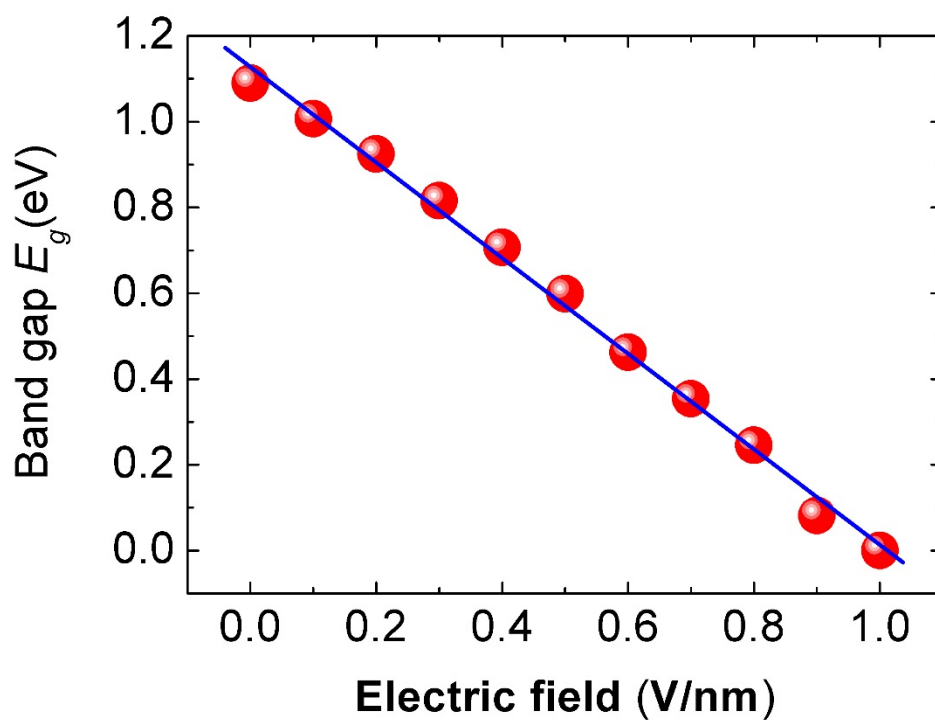
Figure S6. Band gap versus applied electric field for triple-layer MoS$_2$. The red (dotted) and blue (solid line) are the calculated data and fitted line, respectively.

6. Fabrication processing, structure and photoresponse properties of four-layer MoS₂ ferroelectric field effect transistor.
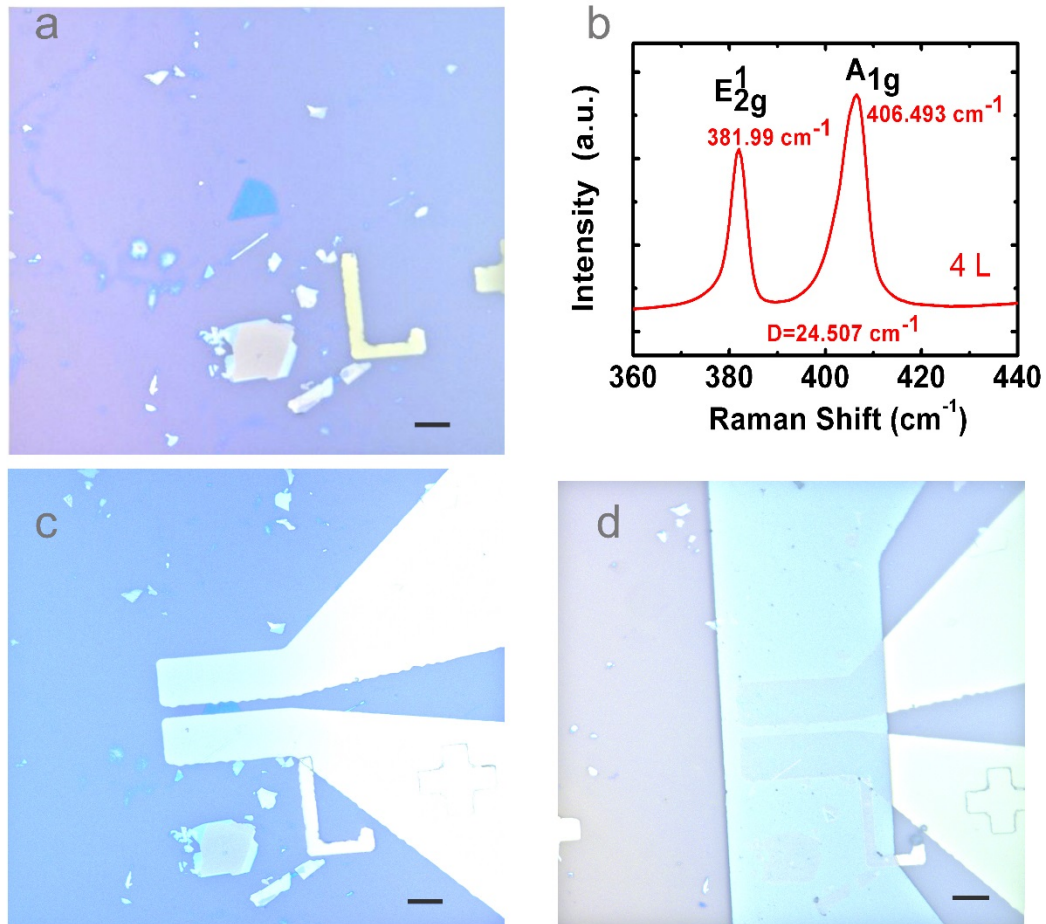

Figure S7. Fabrication and structure of four-layer MoS₂ detector. **a**, Optical image of the four-layer MoS₂. Scale bar, 10μm. **b**, The Raman spectra of the four-layer MoS₂. The peak position of the E_{2g}^1 and A_{1g} are 381.99 cm^{-1} and 406.49 cm^{-1}, respectively. The separation between E_{2g}^1 and A_{1g} modes is approximately 24.50 cm^{-1}. **c**, Optical image of the four-layer MoS₂ on top of a SiO₂-silicon substrate with source and drain (chromium/gold, Cr/Au) electrodes. Scale bar, 10μm. **d**, Optical image of the complete device based on **c**. The device is comprised of four-layer MoS₂ with Cr/Au

contract, 300 nm P(VDF-TrFE) ferroelectric polymer and semi-transparent aluminum

top electrode. Scale bar, 10μm.
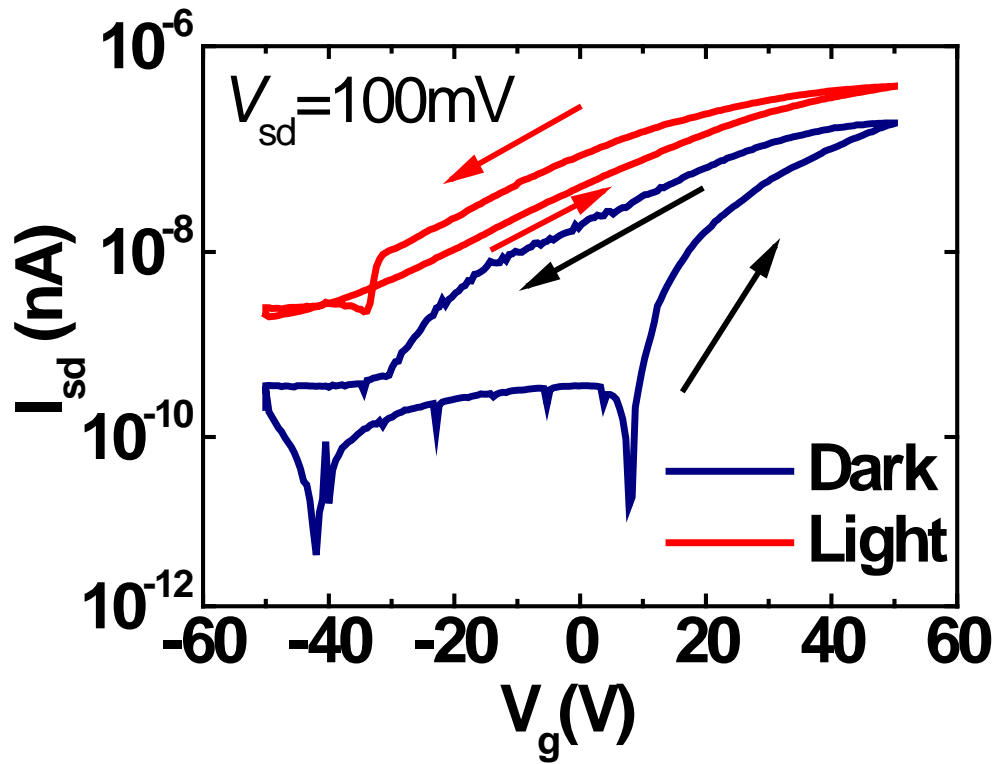
Figure S8. The transfer curves of four-layer MoS_2 photodetector in dark (red line) and

light (blue line) states, respectively. The wavelength of the illumination light is

635nm.

7. Photoresponse properties of ferroelectric polarization gating MoS$_2$ photodetector in the infrared wavelengths
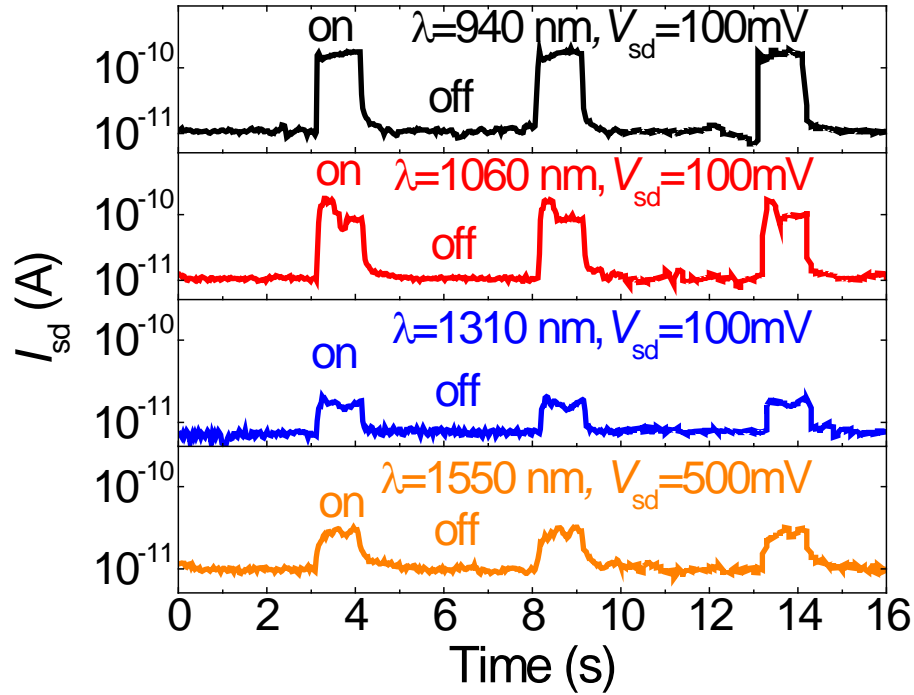

Figure S9. Infrared photoswitching behavior of ferroelectric polarization gating few-layer MoS$_2$ photodetector under 960 nm, 1060 nm, 1310 nm and 1550 nm wavelength laser illuminations, respectively.

8. References

S1   B. Delley, J. Chem. Phys., 2000, **113**, 7756.

S2   J. P. Perdew, K. Burke and M. Ernzerhof, Phys. Rev. Lett., 1996, **77**, 3865.

S3   S. Grimme, J. Comput. Chem., 2006, **27**, 1787.

S4   N. Zibouche, P. Philipsen, A. Kuc and T. Heine, Phys. Rev. B, 2014, **90**, 125440.

Movies

Mov S1

Photoresponse behavior of ferroelectric polarization gated few-layer MoS_2 photodetector under fluorescent lamp illumination.